Dynamic Rupture of Asperities and Stress Change during a Sequence of Large Interplate Earthquakes in the Mexican Subduction Zone

by Takeshi Mikumo, Takashi Miyatake, and Miguel A. Santoyo

Abstract We investigate the spatial and temporal variations of shear stress due to the successive failures over an extensive segment of the Mexican subduction zone during a sequence of large interplate earthquakes that occurred over a period of 13 yr. For this purpose, we develop 3D dynamic rupture models incorporating a shallowly dipping fault located above the subducting plate. The spatial distribution of dynamic stress drop over the fault has been estimated for each of the events, through an inversion procedure using some of the previously derived kinematic fault parameters as observational constraints.

The results revealed quite heterogeneous stress changes during these earthquakes coming from medium to high dynamic stress drop due to the rupture of a few patch-like asperities and from stress increase in between and around them. Two weak asperities located southeast of the Michoacan segment were ruptured first by the 1979 Petatlan event. The 1981 Playa Azul event ruptured two asperities in the central zone with a stress drop higher than 80 bars. The largest 1985 Michoacan earthquake resulted from the rupture of two large-size, strong asperities located at both sides of the 1981 fault zone with high stress drop of 80 to 100 bars and from another two asperities at depth. Two days after this largest event, two asperities were broken during the Zihuatanejo aftershock in the southeastern adjacent zone. Many aftershocks of these large events tend to be distributed in the zones of stress increase outside the asperities, while only small numbers of aftershocks have been observed within these asperity zones. It appears that several major asperities that existed in this extensive segment have been ruptured successively so as to fill unbroken gaps on the plate interface. Thus, the stress change left over from the previous earthquake has dominant effects on the next event in this subduction zone.

Introduction

A number of large to great earthquakes have taken place with a relatively short recurrence time along the Pacific coastal region of Mexico (Singh et al., 1981), where the Cocos plate subducts beneath the North American plate. The subduction zone extends over the entire length of about 1000 km along the Middle America trench from the Jalisco–Colima regions through the Michoacan–Guerrero regions to the Oaxaca region, which appear to be segmented by the Rivera fracture zone, the East Pacific Rise, the Orozco and O'Gorman fracture zones, and the Tehuantepec ridge, respectively (Fig. 1) (Singh and Mortera, 1991). Most of the major earthquakes in this zone are characterized by an underthrusting mechanism with low dip angles and shallow source depths. The low dip of the interplate contact continues to a depth of about 30 km and changes laterally somewhat steeper westward beneath the Rivera plate and eastward beneath the Caribbean plate (Pardo and Suarez, 1995). The shallow maximum depth of thrust faulting is also char-

acteristic of the Mexican subduction zone as compared with that in other subduction zones having similar age and relative convergence velocity (Suarez and Sanchez, 1996).

Of particular importance from the seismotectonic point of view are the large earthquakes that occurred in the northern segments of the subduction zone between the Rivera and Orozco fracture zones. The segments have ruptured in a sequence of six large earthquakes ($7.0 < Ms < 8.1$) over a period of 13 yr from 1973 to 1986: the 1973 Colima earthquake ($Ms = 7.5$) between the Jalisco and Michoacan segments; the 1979 Petatlan earthquake ($Ms = 7.6$) in the western part of the Guerrero segment; the 1981 Playa Azul earthquake ($Ms = 7.3$); the 19 September 1985 Michoacan earthquake ($Ms = 8.1$) and its largest aftershock, the 21 September 1985 Zihuatanejo earthquake ($Ms = 7.6$); and the 1986 earthquake ($Ms = 7.0$) in the Michoacan segment (Table 1). Figure 2 reproduces a map of the rupture zones of these large earthquakes inferred from the distribution of
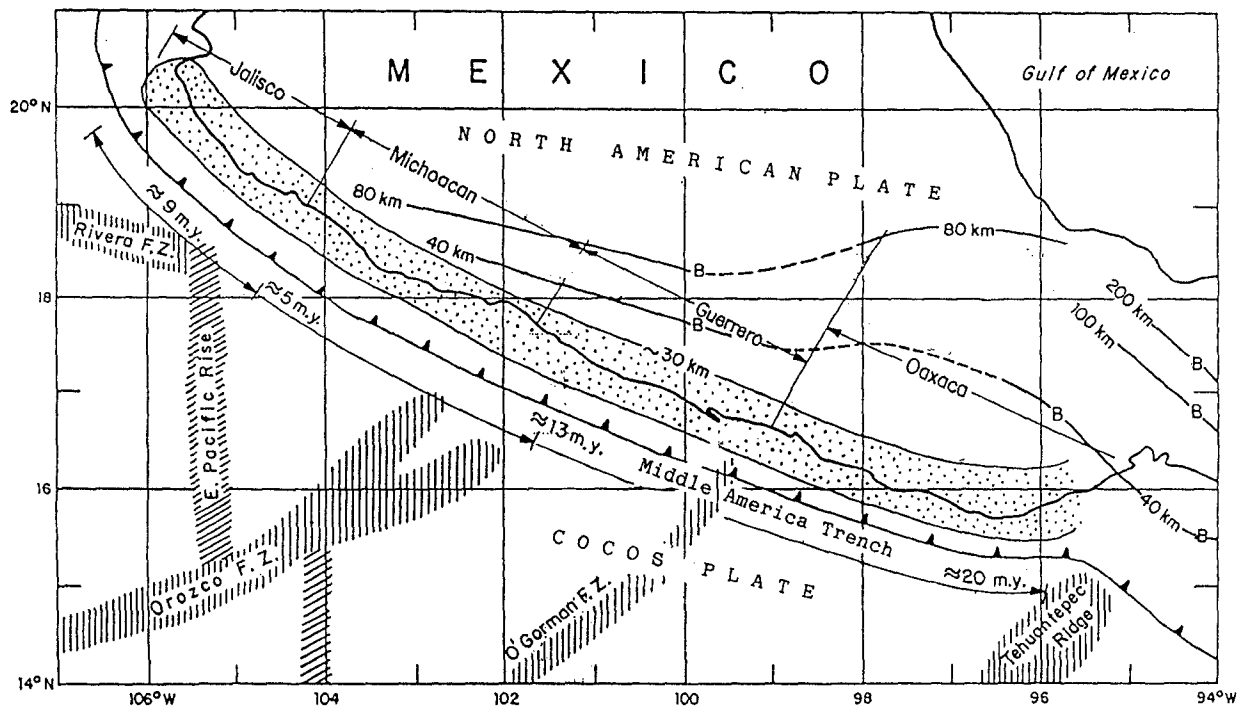
Figure 1.   Tectonic features of the Mexican subduction zones including the Middle America trench, fracture zones, and ridges (modified from Singh and Mortera, 1991). Contours marked B indicate the depth to the upper plane of the Wadati–Benioff zone. The dotted region along the coast shows the zone of strong interface coupling when large thrust earthquakes take place.

Table 1
Recent Major Earthquakes in and around the Michoacan Segment of the Mexican Subduction Zone
(taken from Singh and Mortera, 1991)

Earthquakes	Date	Lat (°N)	Lon (°W)	Ms	M_0 ($\times 10^{28}$ dyn.cm)	Mw
1. Petatlan	03/14/1979	17.46	101.46	7.6	0.55	7.62
2. Playa Azul	10/25/1981	17.75	102.25	7.3	0.85	7.43
3. Michoacan	09/19/1985	18.14	102.71	8.1	3.90	8.05
4. Zihuatanejo	09/21/1985	17.62	101.82	7.6	0.90	7.66
5. Aftershock	04/30/1986	18.42	102.99	7.0	0.30	6.99

their aftershocks (Havskov *et al.*, 1983; UNAM Seismology Group, 1986).

These large earthquakes have been analyzed by a number of investigators from forward modeling or moment-tensor inversion of teleseismic, long-period body and surface waves (e.g., Singh *et al.*, 1984; Astiz *et al.*, 1987; Singh and Mortera, 1991; Ruff and Miller, 1994). These earlier analyses, mostly based on a simple point-source assumption, provided their geometrical source parameters including the source depth, fault strike and dip, and slip angle, as well as the overall source function, seismic moment, and in some cases, average slip and static stress drop. The estimated fault strike and slip angle are generally consistent with the convergence direction between the Cocos–North America plates

predicted from the global plate tectonic models (McNally and Minster, 1981; DeMets *et al.*, 1990; Ruff and Miller, 1994). Recent waveform inversions have revealed more detailed features of four of these large earthquakes. The spatial distribution of slip over the fault plane has been recovered from the inversion for the 1979 Petatlan, 1981 Playa Azul, 1985 Michoacan, and 1985 Zihuatanejo earthquakes, using teleseismic P waves (Mendoza and Hartzell, 1988; Mendoza, 1993, 1995), and particularly for the Michoacan earthquake, using strong-motion velocity records with long- and intermediate-period teleseismic P waves (Mendoza and Hartzell, 1989) and near-source strong-motion records together with coastal surface uplift measurements (Mendez and Anderson, 1991).

Although the previous studies have provided some basic features and kinematic fault models for each of these earthquakes, their dynamic rupture processes and hence the change of stress state due to the successive occurrence of these events have not yet been made clear. Our main purpose in the present article is to elucidate how the spatial and temporal variations of shear stress could occur due to the successive failure on an extensive segment over the large-plate boundary during a sequence of large earthquakes. For this purpose, we develop 3D dynamic rupture models of the four large thrust earthquakes in this subduction zone, incorporating a shallowly dipping fault plane rupturing a part of the interface between the subducting Cocos plate and the over-

(a)

AFTERSHOCKS
20 TO 30 SEP. 1985

$M_c < 3$ x   20 Sep 1985
$3 \leq M_c < 4$ △ $3 \leq M_c < 4$ ▲
$M_c \geq 4$ o $M_c \geq 4$ ●

Strong motion stations ⊕
Portable stations   +

1973
(7.5)

1985
(8.1)

CAL

VIL

UNI

Lázaro Cárdenas

1979
(7.6)

1981
(7.3)

Zihuatanejo   ZIH   Petatlan

1985
(7.5)

Middle America Trench

0   50   100 km

19° N

18°

17°
104° W   103°   102°   101°

(b)

MEXICO

● M<3.0
o M≥3.0
▲ Portable Array
△ Accelerograph

BVT

PDE

Playa Azul   Lázaro Cárdenas

CBZ   PLV   PDE

UON

Foreshocks   2

Main shock

ZIH

1 month aftershock
area of Petatlan
Earthquake

0   50 km

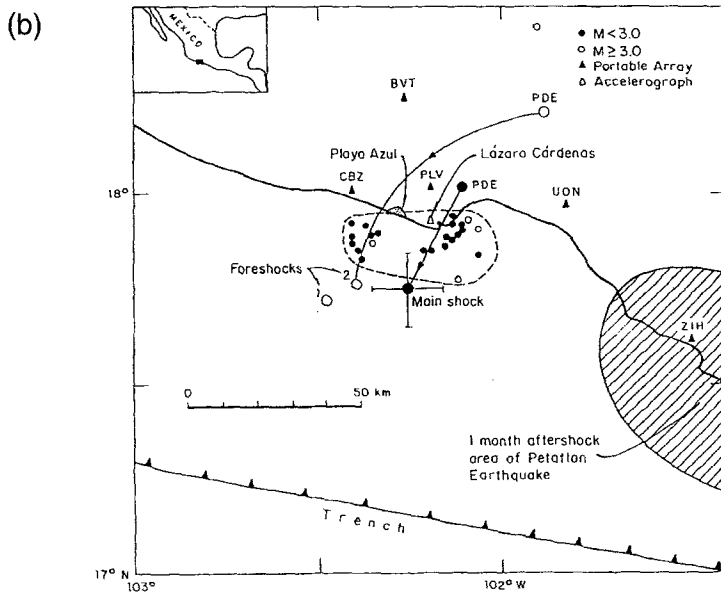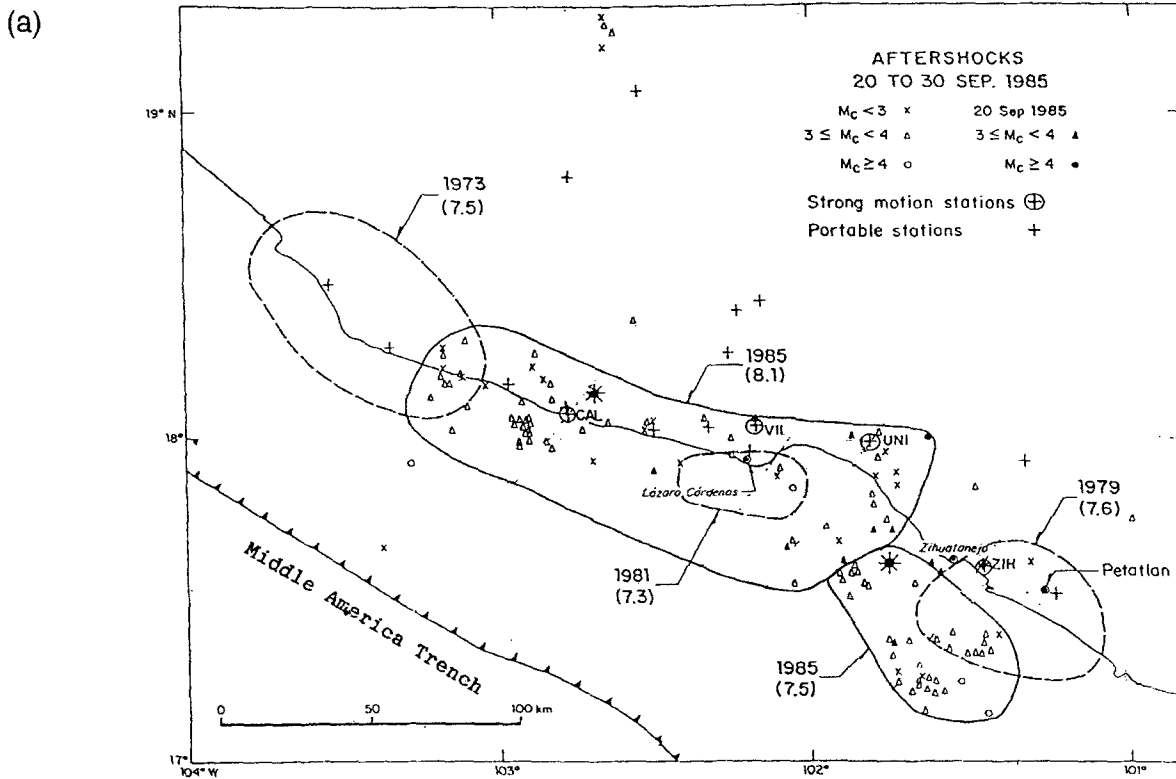Trench

18°

17° N
103°   102° W

Figure 2.   (a) Rupture zones of five large earthquakes in and near the Michoacan segment, inferred from the distribution of aftershocks (UNAM Seismology Group, 1986). (b) Aftershock locations of the 1981 Playa Azul earthquake (Havskov et al., 1983).

riding North America plate. In these models, some of the kinematic fault parameters previously derived from waveform inversion (Mendoza and Hartzell, 1989; Mendoza, 1993, 1995) are used as observational constraints. From this analysis, we obtain spatially heterogeneous static and dynamic stress drops over the fault plane of each earthquake. We will show how dynamic rupture involving that of a few asperities could develop into a large fault zone and how the shear stress increases around and between these asperities. Finally, we will examine how the stress left over from the previous large earthquake have affected the subsequent events under the tectonic stress coming from plate movements.

Method of Dynamic Rupture Modeling

The method of dynamic rupture modeling has been described in Miyatake (1992), Mikumo and Miyatake (1993, 1995), Fukuyama and Mikumo (1993), and Beroza and Mikumo (1996). To deal with dynamic rupture on a dipping

thrust fault, we basically follow the approach taken by Mikumo and Miyatake (1993) with some improvements. Our dynamic model is specified by the spatial distribution of dynamic stress drop and strength excess over the fault, with dynamically calculated source-time functions. We will derive the distribution of these dynamic parameters from the distribution of fault slip and rupture times obtained from the previous kinematic waveform inversion.

The first step in this approach is to construct a 3D dynamic model on the dipping fault plane embedded in a horizontally layered half-space. The dynamic rupture propagating on the fault and all displacement components can be calculated by solving the 3D wave equation with a finite-difference scheme under a fracture criterion and the appropriate boundary conditions. This is actually a 3D shear-crack problem. The fracture criterion applied here is such that the rupture occurs at points when the increasing shear stress due to the approach of the rupture front exceeds the prescribed maximum stress level. The boundary conditions to be satisfied on and across the fault are (1) the initially applied and then increased, tangential shear stress drops immediately to the level of dynamic frictional stress directly above and directly below the dipping fault at the time of rupture, and (2) the normal stress and normal displacement components should be continuous across the fault. Because these boundary conditions can be discretized into finite-difference equations, six displacement components at any point directly above and directly below the fault can be solved in terms of dynamic stress drop in the case of pure thrust faulting (Mikumo and Miyatake, 1993). Other boundary conditions imposed are (a) the stress-free condition on the ground surface, (b) the continuity of all stress and displacement components at each of the layer interfaces (Mikumo *et al.*, 1987), and (c) absorbing boundary conditions to attenuate reflected waves at the bottom and side boundaries of the model space (Levander, 1985).

The second step is to estimate the peak shear stress just before each point on the fault ruptures. The time of rupture can be specified by the arrival time of rupture front from the kinematic waveform inversion (Miyatake, 1992). The strength excess is defined as the difference between the estimated peak shear stress and the initially assumed stress level. However, because the peak shear stress calculated in this way is dependent on the grid spacing and the time increment used in numerical calculations, the estimated strength excess should be regarded as only a lower bound of its real value. In the kinematic fault models obtained for the four target earthquakes, the rupture front was assumed to propagate in a circular shape at a constant velocity. Because this assumption precludes even relative estimates of the peak shear stress over the fault, we will not discuss the absolute values of strength excess in the present article.

The third step is to evaluate the distribution of dynamic stress drop from that of the kinematic fault slip. To do this, we start by estimating local static stress drop in an approximate way, from the formulations given by Okada (1993)

for strains and displacements at depth due to a buried point source in a half-space. By using these approximate estimates as starting values, we calculate dynamic slips over the fault, including the effects of rupture propagation and a horizontally layered structure, and compare them with the kinematic fault slips. The ratio between the kinematic and dynamic slips at each point is then multiplied to the previously estimated stress drop in the next iteration. A nonlinear iterative procedure is applied to minimize the rms difference between the kinematic and dynamic slips within a reasonably small value, and the distribution of dynamic stress drop will be obtained from a best-fitting model.

As a final check, it is hoped to see how well the dynamic models derived could reproduce the waveforms recorded in the near field, as have been done in some previous work (Fukuyama and Mikumo, 1993; Beroza and Mikumo, 1996; Ide and Takeo, 1996), because the slip velocity function and the rise time calculated from the dynamic models are somewhat different from those assumed in the kinematic models. We calculated the synthetic waveforms to compare with the near-source records from the 1985 Michoacan earthquake, and the results will be given in a companion article (Mikumo *et al.*, 1998). However, we did not calculate teleseismic synthetic seismograms, because some difference in the source-time function between dynamic and kinematic models will be masked in long-period, teleseismic *P* waveforms.

The configuration of our dynamic model is taken so as to conform the geometry of the kinematic fault model. Although several moment-tensor inversions gave slightly different dip and strike for each of the earthquakes, the dip is fixed here at 14° for all four events, following Mendoza and Hartzell (1988, 1989) and Mendoza (1993, 1995), which corresponds to the dip of the Wadati–Benioff zone in this region; the fault strike is taken at 300° for three of these earthquakes, with the exception of the 1979 Petatlan earthquake, at 293°, which is close to the orientation of the trench axis in this region (Mendoza, 1993). We assume the slip angle of 90° indicating pure dip-slip motion on a dipping thrust fault for all four events, despite that the 1985 Michoacan earthquake showed small right-lateral strike-slip component (Mendoza and Hartzell, 1989), because they suggested that the small component is not important to the overall character of this earthquake. The fault dimension and the hypocentral depth are taken as exactly the same as those in the kinematic models.

The crust and uppermost mantle structure assumed here (Table 2) is a layered velocity model (Mendoza and Hartzell, 1989) taken from the gradient structure (Stolte *et al.*, 1986) for the Michoacan coastal region. This is similar to the layered velocity model given by Valdez *et al.* (1982, 1986) but somewhat different from their more refined model (Valdez and Meyer, 1996) including the subducting plate overridden by oceanic crusts. The effects of small differences in the velocity structure between the subducted slab and the overlying mantle wedge on dynamic rupture process will be discussed in a separate article (Mikumo *et al.*, 1998), but

Table 2

Crustal Velocity Model Used in This Study
(Mendoza and Hartzell, 1989)

Layer	Vp (km/sec)	Vs (km/sec)	Density (g/cm³)	Top Depth (km)
1	5.80	3.35	2.68	0
2	6.40	3.69	2.78	6
3	7.00	4.04	2.85	25
4	8.00	4.62	3.00	35

they do not seem very significant if the velocity contrast is within 20%.

For numerical calculations by a finite-difference scheme, the grid spacing and the time increment should be taken so as to satisfy the stability condition for 3D wave propagation. In the present case, the fault dimension of the four large earthquakes exceeds several tens to even 180 km, and their overall rupture duration ranges between 25 and 60 sec. To save the number of grids and the computation time, the dimensions of the model space, the crust and upper mantle structure, and the fault size under calculation, all have been reduced proportionally to 1/10 of their actual dimensions. Keeping the stability condition ($Vs \cdot dt/dh \leqq 1/2$) with the given velocity values, the time increment and the overall rupture duration can also be reduced to 1/10. Since the stress drop to give the same average slip is inversely proportional to the square root of the fault area, the dynamic stress drop from this calculation has also been reduced to 1/10 to get their correct estimates. For the 1979 Petatlan and 1985 Michoacan earthquakes, we take the grid spacing $dh = 1.0$ km and the time increment $dt = 0.02$ sec, while for the 1981 Playa Azul and 1985 Zihuatanejo events, $dh = 0.5$ km and $dt = 0.01$ sec. These correspond to $dh = 10$, or 5 km, and $dt = 0.2$, or 0.1 sec, in actual cases, respectively. The dimensions of the 3D model space in these cases are 750 × 180 × 580 km and 375 × 80 × 290 km, respectively, and the total number of grid points is about 227,000, and the total time step of 500 covers 100 and 50 sec, respectively.

Dynamic Rupture Processes of Four Large Thrust Earthquakes

The Petatlan Earthquake of 14 March 1979 (Ms = 7.6)

The Petatlan earthquake occurred in the subduction zone off the coast between Michoacan and Guerrero. This region had been quiet since 1943, but after this earthquake, a sequence of large to great thrust earthquakes successively took place in the northwestern part of this region. A number of aftershocks located by the local seismic network indicate that the Petatlan mainshock occurred on the upper interface of the subducting Cocos plate (Valdez and Meyer, 1996).

The point-source parameters of this earthquake have been estimated from P and Rayleigh waves recorded at IDA,

WWSSN, and other stations (Chael and Stewart, 1982; Singh and Mortera, 1991; Ruff and Miller, 1994). The spatial distribution of coseismic slip has been inferred from teleseismic P waves recorded at the GDSN broadband network and WWSSN stations, using a linear finite-fault inversion scheme (Mendoza, 1995), under a constant rupture velocity of 3.3 km/sec and with five consecutive 1-sec boxcar source-time functions. The coseismic slip calculated over the fault dimension of 120 × 120 km covering depths from 2 to 30 km shows a small zone with a peak slip of 70 cm near the hypocenter and a large-size zone of a maximum of 1.2 m farther southeast (Mendoza, 1995), as reproduced in Figure 3a.

Figure 3b shows the distribution of static stress drop calculated from the fault slip given in Figure 3a (Mendoza, 1995). In the corresponding dynamic model, we take the rupture starting point at a depth of 15 km, following Mendoza (1995). The dynamic stress-drop distribution including the effects of rupture propagation is shown in Figure 3c. Although the general pattern is quite similar to that in 3b, the zone of positive stress drop is slightly more concentrated than for the static case. We notice that local stress drop of 5 to 10 bars southeast of the hypocenter generated relatively large slip with a maximum of 1.2 m and that the medium slip (70 cm) around the hypocenter comes from a small positive stress drop. Zones of negative stress drop extend over the surrounding area except near the northwestern deeper section.

The estimated strength excess (not shown here) is not large but tends to have slightly higher values in the negative stress-drop zone, while it is smaller near the hypocenter and in the central portion of the high stress-drop zone. Figures 3d and 3e compare the distribution of final fault slip derived from kinematic waveform inversion (Mendoza, 1995) with that of the dynamic slip at 100 sec after the initiation of rupture calculated from the final dynamic model. The rms difference between the dynamic and kinematic slip is 5.9 cm. It seems that the dynamic model derived under a constant rupture velocity well reproduces the slip patterns, although the seismic moment 1.97×10^{27} dyne cm is slightly larger than 1.5×10^{27} dyne cm in the kinematic model. It should be emphasized that relatively large slip shown here results from a dynamic stress drop of less than 10 bars. The small zones of positive stress drop may thus be regarded as real asperities.

The Playa Azul Earthquake of 25 October 1981 (Ms = 7.3)

This interplate earthquake took place within the central portion of the Michoacan segment and is located between the source regions of two subsequent large events in 1985, the 19 September Michoacan and 21 September Zihuatanejo earthquakes. The centroid source parameters of this earthquake have been estimated from body and surface waves (Dziewonski and Woodhouse, 1983; Havskov et al., 1983; LeFevre and McNally, 1985; Zhang and Kanamori, 1988; Priestley and Masters, 1986; Astiz et al., 1987; Singh and

1979 PETATLAN EARTHQUAKE

(a) SLIP DISTRIBUTION (cm)

SE   NW

DISTANCE DOWN DIP (KM) — 0, 30, 60, 90, 120

DEPTH (KM) — 2, 8, 14, 20, 26

119   *70   25

20 KM

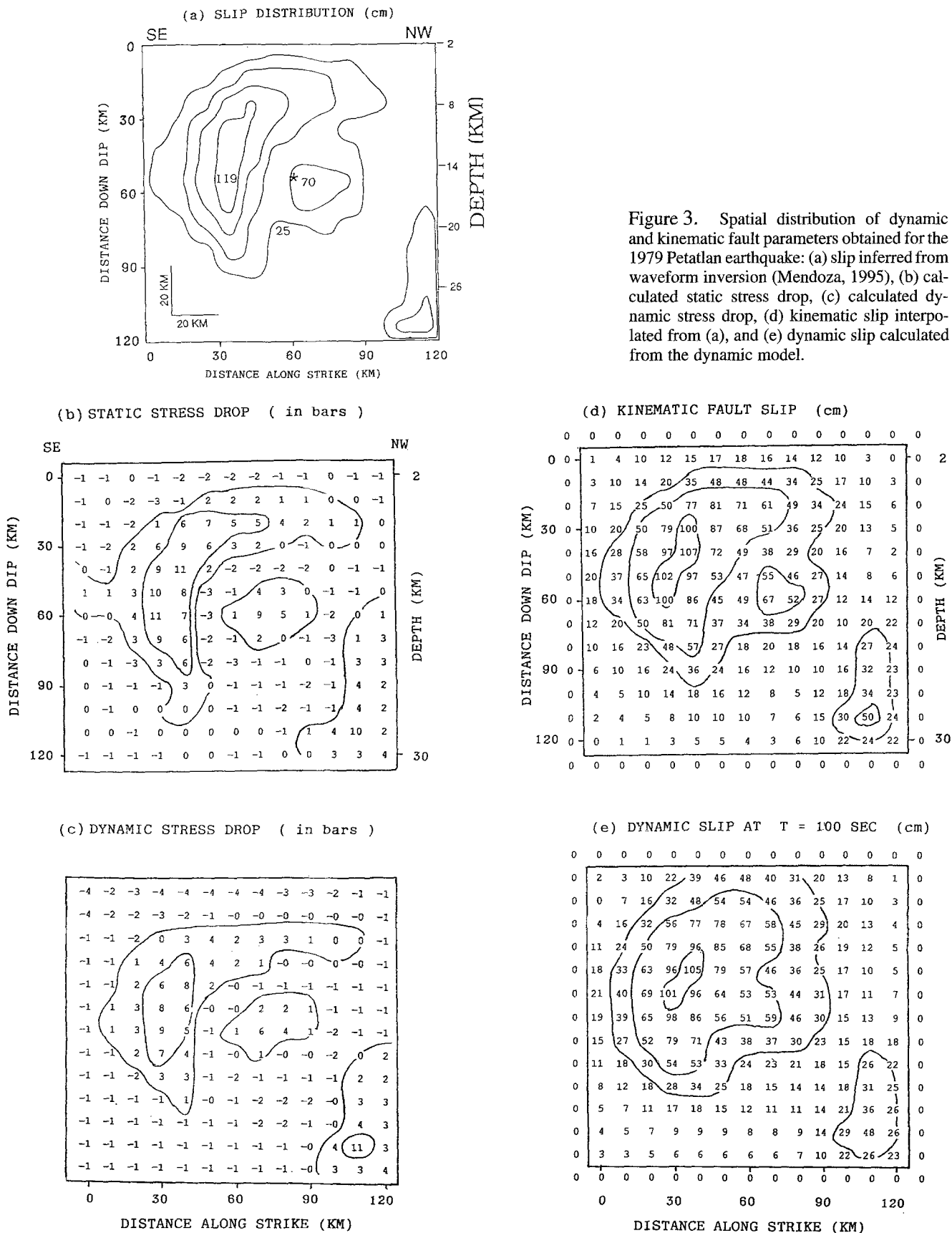DISTANCE ALONG STRIKE (KM) — 0, 30, 60, 90, 120

Figure 3. Spatial distribution of dynamic and kinematic fault parameters obtained for the 1979 Petatlan earthquake: (a) slip inferred from waveform inversion (Mendoza, 1995), (b) calculated static stress drop, (c) calculated dynamic stress drop, (d) kinematic slip interpolated from (a), and (e) dynamic slip calculated from the dynamic model.

(b) STATIC STRESS DROP (in bars)

SE   NW

```
-1  -1   0  -1  -2  -2  -2  -2  -1  -1   0  -1  -1
-1   0  -2  -3  -1   2   2   2   1   1   0   0  -1
-1  -1  -2   1   6   7   5   5   4   2   1   1   0
-1  -2   2   6   9   6   3   2   0  -1   0   0   0
 0  -1   2   9  11   2  -2  -2  -2  -2   0  -1  -1
 1   1   3  10   8  -3  -1   4   3   0  -1  -1   0
 0   0   4  11   7  -3   1   9   5   1  -2   0   1
-1  -2   3   9   6  -2  -1   2   0  -1  -3   1   3
 0  -1  -3   3   6  -2  -3  -1  -1   0  -1   3   3
 0  -1  -1  -1   3   0  -1  -1  -1  -2  -1   4   2
 0  -1   0   0   0   0  -1  -1  -2  -1  -1   4   2
 0   0  -1   0   0   0   0   0  -1   1   4  10   2
-1  -1  -1  -1   0   0  -1  -1   0   0   3   3   4
```

DISTANCE DOWN DIP (KM) — 0, 30, 60, 90, 120

DEPTH (KM) — 2, 30

(c) DYNAMIC STRESS DROP (in bars)

```
-4  -2  -3  -4  -4  -4  -4  -4  -3  -3  -2  -1  -1
-4  -2  -2  -3  -2  -1  -0  -0  -0  -0  -0  -0  -1
-1  -1  -2   0   3   4   2   3   3   1   0   0  -1
-1  -1   1   4   6   4   2   1  -0  -0   0  -0  -1
-1  -1   2   6   8   2  -0  -1  -1  -1  -1  -1  -1
-1   1   3   8   6  -0  -0   2   2   1  -1  -1  -1
-1   1   3   9   5  -1   1   6   4   1  -2  -1  -1
-1  -1   2   7   4  -1  -0   1  -0  -0  -2   0   2
-1  -1  -2   3   3  -1  -2  -1  -1  -1  -1   2   2
-1  -1  -1  -1   1  -0  -1  -2  -2  -2  -0   3   3
-1  -1  -1  -1  -1  -1  -1  -2  -2  -1  -0   4   3
-1  -1  -1  -1  -1  -1  -1  -1  -1  -0   4  11   3
-1  -1  -1  -1  -1  -1  -1  -1  -1.  -0   3   3   4
```

0   30   60   90   120

DISTANCE ALONG STRIKE (KM)

(d) KINEMATIC FAULT SLIP (cm)

```
0   0   0   0   0   0   0   0   0   0   0   0   0   0   0
1   4  10  12  15  17  18  16  14  12  10   3   0   0   2
3  10  14  20  35  48  48  44  34  25  17  10   3   0
7  15  25  50  77  81  71  61  49  34  24  15   6   0
10  20  50  79 100  87  68  51  36  25  20  13   5   0
16  28  58  97 107  72  49  38  29  20  16   7   2   0
20  37  65 102  97  53  47  55  46  27  14   8   6   0
18  34  63 100  86  45  49  67  52  27  12  14  12   0
12  20  50  81  71  37  34  38  29  20  10  20  22   0
10  16  23  48  57  27  18  20  18  16  14  27  24   0
6  10  16  24  36  24  16  12  10  10  16  32  23   0
4   5  10  14  18  16  12   8   5  12  18  34  23   0
2   4   5   8  10  10  10   7   6  15  30  50  24   0
0   1   1   3   5   5   4   3   6  10  22  24  22   0  30
0   0   0   0   0   0   0   0   0   0   0   0   0   0   0
```

DISTANCE DOWN DIP (KM) — 0, 30, 60, 90, 120

DEPTH (KM) — 2, 30

(e) DYNAMIC SLIP AT T = 100 SEC (cm)

```
0   0   0   0   0   0   0   0   0   0   0   0   0   0   0
2   3  10  22  39  46  48  40  31  20  13   8   1   0
0   7  16  32  48  54  54  46  36  25  17  10   3   0
4  16  32  56  77  78  67  58  45  29  20  13   4   0
11  24  50  79  96  85  68  55  38  26  19  12   5   0
18  33  63  96 105  79  57  46  36  25  17  10   5   0
21  40  69 101  96  64  53  53  44  31  17  11   7   0
19  39  65  98  86  56  51  59  46  30  15  13   9   0
15  27  52  79  71  43  38  37  30  23  15  18  18   0
11  18  30  54  53  33  24  23  21  18  15  26  22   0
8  12  18  28  34  25  18  15  14  14  18  31  25   0
5   7  11  17  18  15  12  11  11  14  21  36  26   0
4   5   7   9   9   9   8   8   9  14  29  48  26   0
3   3   5   6   6   6   6   6   7  10  22  26  23   0
0   0   0   0   0   0   0   0   0   0   0   0   0   0   0
```

0   30   60   90   120

DISTANCE ALONG STRIKE (KM)

Mortera, 1991; Ruff and Miller, 1994). Teleseismic *P* waves recorded at GDSN and WWSSN stations were used for source inversion to recover slip distribution on the fault. A linear waveform inversion has been applied (Mendoza, 1993), with a triangular source-time function of 1-sec duration and a constant rupture velocity of 2.6 km/sec starting from the hypocenter at a 14-km depth, for two data sets corresponding to the arrival times of small initial *P* phase (m2) and of major *P*-wave energy (*MS*). The distributions of fault slip over a dimension of 60 × 70 km covering depths between 6 and 23 km (Mendoza, 1993) are reproduced in Figure 4a for the *MS* solution. The slip indicates a concentrated distribution within a narrow zone with a radius of about 10 km located in the downdip section at depths between 13 and 20 km. The maximum slip in the main source region exceeds 3.5 m and is about 1 m in the updip region.

Figure 4b shows the distribution of static stress drop calculated from the fault slip given in 4a (Mendoza, 1993). For the corresponding dynamic model, we included the rupture propagation as in the previous case. The pattern of dynamic stress drop shown in 4c appears quite similar to the static case (4b). It is found that high stress drop exceeding 50 bars with a maximum of 94 bars is the source generating the large slip concentrated in the downdip section and that medium stress drop with 15 to 20 bars corresponds to the isolated large-slip zone in the shallower fault section. Again, these high stress-drop zones are surrounded by negative stress drop covering the remaining part of the fault. Quite large, negative stress drop can be identified between the medium stress drop in the updip and the high stress drop in the downdip sections. This suggests that the failure of two separated asperities caused this earthquake, and then the shear stress in this interstitial zone and the surrounding areas increased after the rupture. The strength excess (not shown here) has relatively large values in this zone and in the deepest fault section just below the high stress-drop zone. These zones would have delayed rupture propagation if a nonuniform rupture velocity had been assumed.

The distribution of dynamic slip at 35 sec after the rupture initiation that has been calculated from the final dynamic model are compared with that of final fault slip derived from kinematic inversion (Mendoza, 1993) in Figures 4d and 4e. The rms difference between the dynamic and kinematic slips over the fault is 4.8 cm, suggesting that the present dynamic model could reproduce the slip patterns quite well. The total seismic moment calculated here is 8.7 × 10^{26} dyne cm, while it is 7.1 × 10^{26} dyne cm in the kinematic model.

The Michoacan Earthquake of 19 September 1985 (*Ms* = 8.1)

This was the largest earthquake that occurred in the Mexican subduction zone since the 1932 Jalisco earthquake (*Ms* = 8.2) and ruptured the Michoacan segment of the Cocos–North America plate boundary over at least 150 km, causing heavy damage in the Valley of Mexico. The source

parameters of this unusually large earthquake have been estimated from a number of observations mainly by body and surface waves (Anderson *et al.*, 1986; UNAM Seismology Group, 1986; Eissler *et al.*, 1986; Ekstrom and Dziewonski, 1986; Houston and Kanamori, 1986; Riedesel *et al.*, 1986; Priestley and Masters, 1986; Astiz *et al.*, 1987; Singh *et al.*, 1988; Singh and Mortera, 1991; Ruff and Miller, 1994). Several analyses indicate that the mainshock consisted of two subevents, each with the average duration of 12 to 16 sec separated by about 25 to 28 sec, suggesting that the second subevent occurred about 70 to 95 km southeast of the first event. The average rupture velocity between the two sources ranged from 2.0 to 2.8 km/sec propagating toward the direction of 97° to 100°. The dimension of the rupture zone has been estimated from the extent of aftershock area as about 170 × 50 km (Fig. 2a), and the average slip as of the order of 2.2 m (UNAM Seismology Group, 1986) and 4.3 m (Ruff and Miller, 1994). An attempt was also made to simulate the recorded near-field displacements by a 2D cracklike model (Yomogida, 1988).

A linear least-squares waveform inversion of near-source strong-motion records and teleseismic *P* waves has been made (Mendoza and Hartzell, 1989) to recover the slip distribution on the fault plane with a dimension of 180 × 140 km covering a depth range of 6 to 40 km and with a hypocentral depth of 17 km. Rupture was assumed to propagate at a constant velocity of 2.6 km/sec, with a 2-sec triangular source-time function. The results, as reproduced in Figure 5a, indicate the existence of three major sources of predominantly dip-slip motion: (1) a peak slip of 6.5 m in a region of 80 × 55 km near the hypocenter, (2) a peak slip of 5 m in a 45 × 60 km area on the southeast portion 70 km away from the hypocenter at depths between 10 and 24 km, and (3) a peak slip of 3 m in a 30 × 60 km area at depths between 27 and 39 km (Mendoza and Hartzell, 1989). On the other hand, a frequency-domain inversion (Mendez and Anderson, 1991), using surface static displacements recovered from strong-motion records and coastal uplift, indicates two areas of high slip velocity and large slip, one located downdip of the hypocenter with a slip exceeding 3 m and the other with a 4-m slip, which are separated from each other by about 100 km.

In the dynamic model that follows, we refer to the results given by Mendoza and Hartzell (1989), to compare with those obtained by the same technique for the other three earthquakes. Figure 5b provides the static stress-drop distribution calculated from the distribution of final slip (Mendoza and Hartzell, 1989) shown in Figure 5a. Note that the distribution involves three high stress-drop zones nearly corresponding to the large-slip zones and wide negative zones separating the positive zones. The distribution of dynamic stress drop shown in Figure 5c, which included the effects of coherent rupture propagation and were calculated for a horizontally layered structure, still retains the general pattern similar to 5c. We notice that high stress drop with a maximum of 100 bars near the rupture nucleation point yielded

1981 PLAYA AZUL EARTHQUAKE
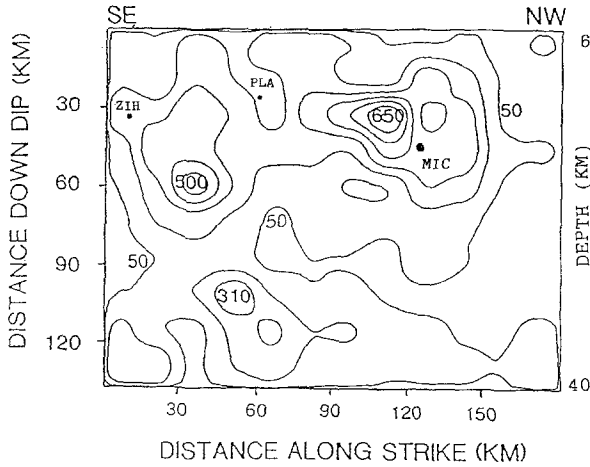

(a) SLIP DISTRIBUTION (cm)

Figure 4. Spatial distribution of dynamic and kinematic fault parameters obtained for the 1981 Playa Azul earthquake: (a) slip inferred from waveform inversion (Mendoza, 1993), (b) calculated static stress drop, (c) calculated dynamic stress drop, (d) kinematic slip interpolated from (a), and (e) dynamic slip calculated from the dynamic model.


(b) STATIC STRESS DROP (in bars)

(c) DYNAMIC STRESS DROP (in bars)

(d) KINEMATIC FAULT SLIP (cm)

(e) DYNAMIC SLIP AT T = 35 SEC (cm)

Figure 5. Spatial distribution of dynamic and kinematic fault parameters obtained for the 1985 Michoacan earthquake: (a) slip inferred from waveform inversion (Mendoza and Hartzell, 1989)—solid circles marked by PLA and ZIH indicate the hypocenters of the 1981 Playa Azul and 1985 Zihuatanejo earthquakes, (b) calculated static stress drop, (c) calculated dynamic stress drop, (d) kinematic slip interpolated from (a), and (e) dynamic slip calculated from the dynamic model.
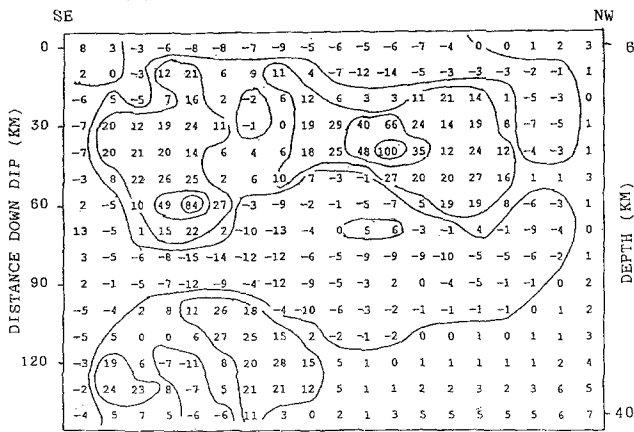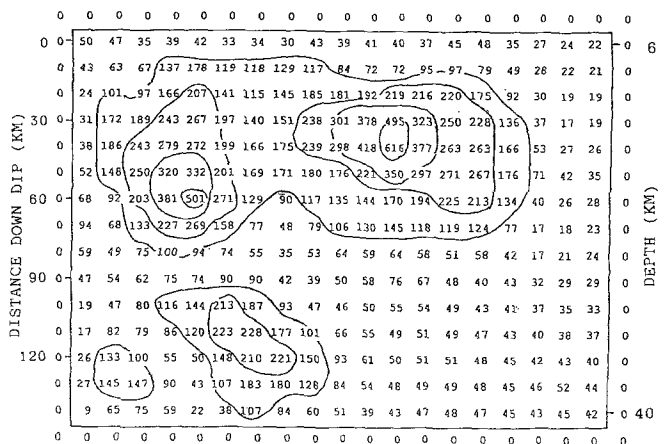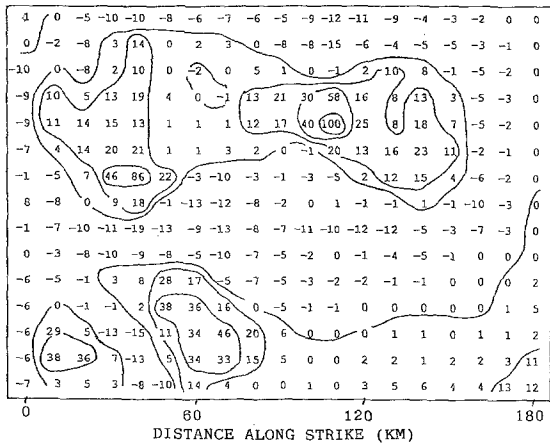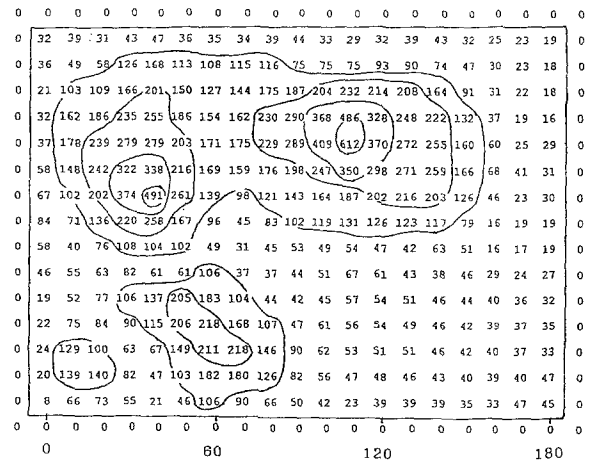
an extremely large slip exceeding 6 m at depths between 10 and 18 km. This may be the failure of the largest asperity at the first stage. The second subevent with a peak slip of 5 m located about 70 km southeast of the first one came from local dynamic stress drop larger than 80 bars, and the third subevent occurred with a stress drop of about 40 bars in the downdip fault section, giving a peak slip of 3 m. While the first and second high stress-drop zones are separated by a zone of small positive stress, the total area extending over 140 km is surrounded by negative stress-drop zones. The third medium stress-drop zone in the deepest fault section is isolated by negative stress drops from the shallower high stress-drop zones. The negative stress drop may be a natural consequence that could occur outside the positive, high stress-drop zone and the peripheral zone of the fault area.

The estimated strength excess (not shown here) has relatively large values in the shallow section above the first high stress-drop zone, the mid-depth southeast of the second one, and the deep zone below the third one. On the other hand, it has lower values between these zones, including around the hypocenter. This would suggest that the rupture starting from the hypocenter propagated southeastward to the second high stress-drop zone without receiving strong resistance. Figures 5d and 5e show the distribution of the kinematic slip interpolated from the results by Mendoza and Hartzell (1989) and the dynamic slip at 100 sec after the initiation of rupture calculated from the present dynamic model. The rms difference between the kinematic and dynamic slips is 7.7 cm, indicating that the slip patterns in the two models are essentially similar. It should be mentioned that large slip exceeding 160 cm can also be observed between the first and second sources where only small stress drop occurred, and that medium slip between 30 and 60 cm occurred over the negative stress-drop zones.

The Zihuatanejo Earthquake of 21 September 1985 ($Ms = 7.6$)

This earthquake occurred 2 days later as the largest aftershock immediately to the southeast of the source region of the 19 September earthquake (Fig. 2a). The centroid source parameters determined by several investigators (Dziewonski and Woodhouse, 1986; Eissler et al., 1986; Priestley and Masters, 1986; Riedesel et al., 1986; Ruff and Miller, 1994) were almost the same as those of the mainshock. The dimension of the ruptured area and the average slip have been estimated as about 60 km × 30 km and 3.3 m (UNAM Seismology Group, 1986). Both teleseismic P and SH waves well recorded at GDSN stations were used in the waveform source inversion (Mendoza, 1993). The inversion was made with the same source-time function and the rupture velocity as in the case of the 1981 Playa Azul earthquake. Figure 6a reproduces the distribution of fault slip (Mendoza, 1993) over a dimension of 90 × 90 km with the hypocentral depth of 20 km. The slip occurs in a circular zone with a radius of about 30 km extending over depths between 12 and 26 km. The maximum slip exceeds 1.7 and

2.0 m for the updip and downdip portions southeast of the hypocenter.

For the dynamic model, we take a slightly smaller fault size of 70 × 80 km than that of the kinematic fault model, because fault slip in the southeast and downdip sections has very small values. This would not give significant effects in estimating stress-drop values. Figure 6b gives the distribution of static stress drop calculated from that of final fault slip (Mendoza, 1993) shown in 6a. The corresponding dynamic stress-drop distribution, which includes the effects of rupture propagation, is shown in Figure 6c. The pattern of dynamic stress drop shows somewhat different features particularly near the upper and lower edges of the fault zone. This may be due to an edge effect during dynamic rupture propagation. It is found that medium stress drop higher than 20 bars in two patches yielded fault slip larger than 170 cm in the central zone of the fault, and hence, these asperities may be the source of this earthquake. This nearly circular, positive stress-drop zone is again surrounded by negative stress drops covering the remaining part of the fault.

The estimated strength excess (not shown here) has relatively high values in part of the updip section just above the positive stress-drop zone and in the downdip section covering part of the central zone. Figures 6d and 6e compare the distribution of final slip obtained from the kinematic inversion (Mendoza, 1993) with that of dynamic slip calculated from the present dynamic model. Although the absolute values at several points slightly differ from each other, their general slip patterns have similar features. The rms difference between the dynamic and kinematic slips is 5.8 cm. The seismic moment 1.64×10^{27} dyne cm in the dynamic model is slightly larger than 1.35×10^{27} dyne cm in the kinematic model.

Uncertainties

The dynamic models for the four earthquakes considered here have been derived with some observational constraints consistent with the corresponding kinematic fault models (Mendoza and Hartzell, 1989; Mendoza, 1993, 1995). The nonlinear iterative inversion procedure used here implies that some uncertainties involved in the calculated kinematic slip would affect almost linearly the estimates of dynamic stress drop. The kinematic waveform inversion mentioned here assumes a constant rupture velocity. Because the rupture time has a strong nonlinear effect on the recorded waveforms, it is possible that this simplified assumption would have affected the kinematic fault slip to some extent and, hence, the dynamic stress drop. Also, a simple source-time function with a constant rise time was used in the kinematic inversion, while the slip-rate source function in dynamic models has nearly an inverse square-root time dependence depending on the location on the fault. Actually, waveform inversion incorporating the dynamically derived slip-rate time functions have yielded a more concentrated distribution of dynamic stress drop than that derived from conventional kinematic inversion (Beroza and

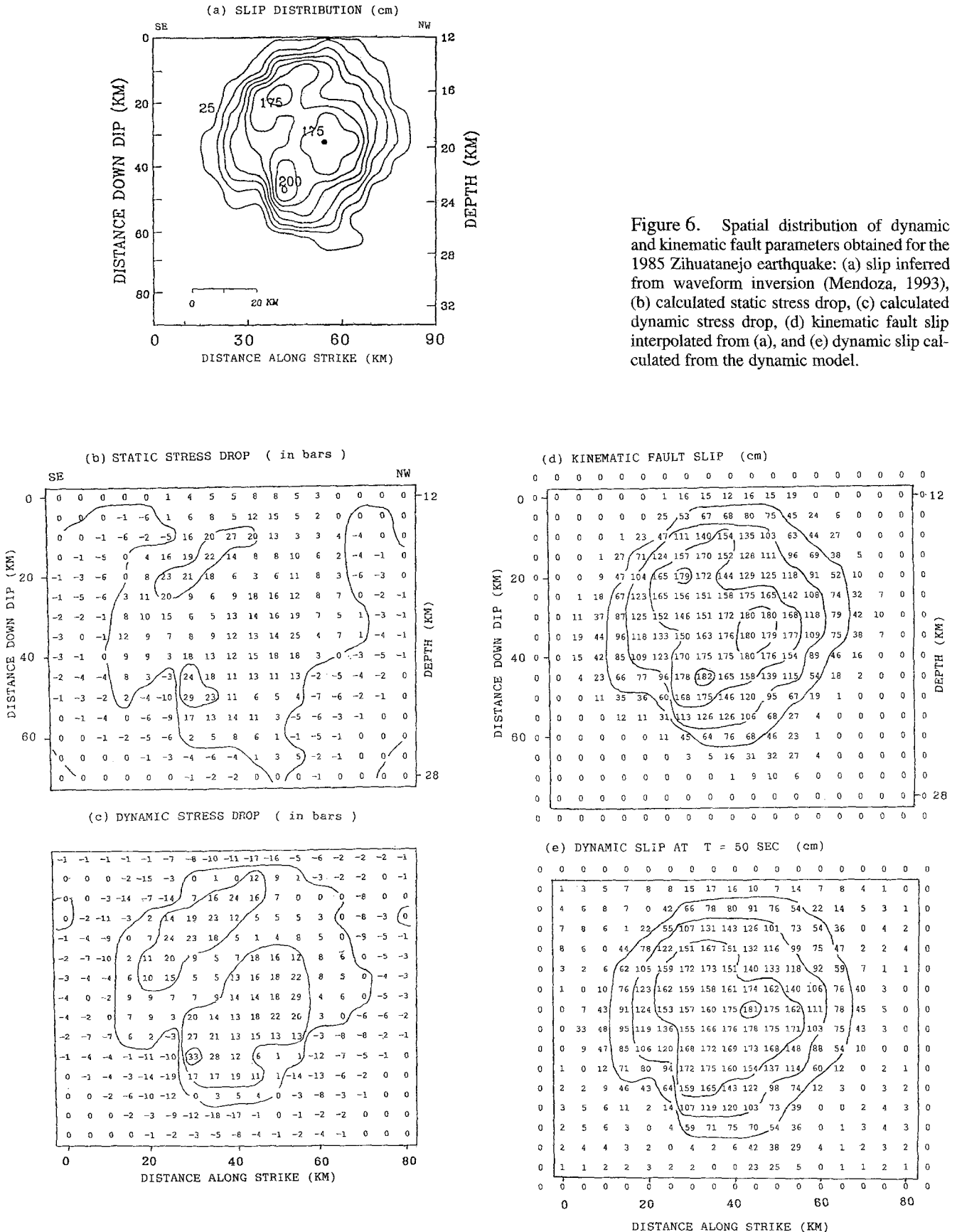**1985 ZIHUATANEJO EARTHQUAKE**

(a) SLIP DISTRIBUTION (cm)

Figure 6. Spatial distribution of dynamic and kinematic fault parameters obtained for the 1985 Zihuatanejo earthquake: (a) slip inferred from waveform inversion (Mendoza, 1993), (b) calculated static stress drop, (c) calculated dynamic stress drop, (d) kinematic fault slip interpolated from (a), and (e) dynamic slip calculated from the dynamic model.

(b) STATIC STRESS DROP (in bars)

(d) KINEMATIC FAULT SLIP (cm)

(c) DYNAMIC STRESS DROP (in bars)

(e) DYNAMIC SLIP AT T = 50 SEC (cm)

Mikumo, 1996). Some difference in the velocity structure between the subducting plate and the overriding mantle wedge could also slightly affect dynamic stress drop on a dipping thrust fault. Thus, the absolute values and even the distribution pattern of dynamic stress drop obtained here could be subjected to minor changes (say, about 10%) if the above conditions are taken into consideration. However, it would be interesting to compare the general pattern of stress drop with aftershock distribution from each of the four earthquakes analyzed here, and also to discuss the spatial and temporal variations of shear stress over an extensive segment of the plate boundary.

Stress Drop and Aftershock Distribution

Now, we compare the general pattern of stress drop during each earthquake with the distribution of its aftershocks. Because the earthquake epicenters in this region determined only from teleseismic observations such as given in the ISC and PDE catalogs are often displaced by 30 to 40 km northeast of those from local and regional networks (e.g., Havskov *et al.*, 1983; Ruff and Miller, 1994), we refer only to the epicentral locations determined by the local seismic network.

The locations of aftershocks of the 1979 Petatlan earthquake have been determined (Valdez and Meyer, 1996; not shown here) by the mobile seismic stations. It does not appear that these aftershock distributions can be correlated with any stress-drop zones (Figs. 3a and 3b), unlike the case of the following three large events. This might be due to much smaller stress drops (<10 bars) in this case. Figure 2b shows the locations of the mainshock and aftershocks of the 1981 Playa Azul earthquake (Havskov *et al.*, 1983), which have been obtained for the first 6 days by a portable seismograph array and a strong-motion station in this region. The aftershocks cluster in the eastern and western sides of the zone delineated by a dotted curve, while there is a gap just north of the mainshock epicenter. The gap corresponds exactly to the high stress-drop zone in the downdip section (Figs. 4b and 4c) just below the hypocenter, suggesting that the large drop of stress could not generate aftershocks in this zone. On the other hand, it is noticed that the increase of stress in the eastern and western sides of the foregoing zone was capable of generating these aftershocks.

Figure 2a gives the locations of the mainshock and aftershocks of the 1985 Michoacan and Zihuatanejo earthquakes (UNAM Seismology Group, 1986). All the locations have been obtained from a portable seismograph array and strong-motion stations in this region for the data during 10 days after the second event. Aftershocks of the first event are distributed nearly in the northwestern section of the mainshock epicenter as well as in the southeastern end region, but only small numbers of aftershocks have been located in the central zone. Because the region northwest of the epicenter and near the southeastern end zone had encountered negative stress drop or only small positive stress

drops (Figs. 5b and 5c), these aftershocks may have been caused by stress increase or the deficit of stress decrease. In the zone just southeast of the epicenter and in the rupture zone of the 1981 Playa Azul earthquake, there was large stress drop, which could not generate many aftershocks. Aftershocks of the second event occurred southwest of the mainshock and mainly in the southeastern region, while almost none was observed around the epicenter. Again, it appears that the increase of stress after the mainshock in the southwest and southeast regions (Figs. 6b and 6c) have generated many aftershocks, while the medium stress drop around the epicenter did not generate aftershocks.

Failure of Asperities and Stress Change over an Extensive Segment

A sequence of the four earthquakes in the Michoacan–western Guerrero segment appear to have taken place on parts of nearly the same interface between the subducting Cocos plate and the overriding North American plate. Figures 7 and 8 accommodate the fault planes of these earthquakes projected onto this interface. Because the initial shear stress prior to the 1979 first event may not be uniformly distributed on the interface, we are looking only at the change of stress state due to the sequence of these earthquakes. Figure 7 shows the zones of positive stress drops higher than 10 bars. Letters PET, PLA, MIC, and ZIH indicate the rupture starting points (i.e., the hypocenters) of the 1979 Petatlan, 1981 Playa Azul, 1985 Michoacan, and 1985 Zihuatanejo earthquakes, and contours with different symbols show dynamic stress drop during these events. We see that these stress-drop zones are distributed like patches over an extensive area but overlapped only on a small area of the 1981 Playa Azul and 1985 Zihuatanejo fault zones. If, however, we take stress-drop zones with higher than 15 bars, these zones are not overlapped but just adjacently located. On the other hand, fault slips from the four earthquakes overlap in several areas: the northwestern part of the fault zone of the 1979 Petatlan earthquake reslipped during the 1985 Michoacan and Zihuatanejo earthquakes, the fault zone of the 1981 Playa Azul earthquake also slipped again during the two 1985 events, and the southeastern part of the fault zone of the Michoacan earthquake appears to have reslipped during its largest aftershock (see, Mendoza, 1993, 1995).

If we define here an asperity as part of the fault zone having medium to high positive stress drops, for example, higher than 10 to 15 bars, we identify one asperity for the Petatlan earthquake, two asperities with one having 80 bars stress drop for the Playa Azul earthquake, four large asperities with two having 80 to 100 bars stress drop for the Michoacan earthquake, and two asperities for the Zihuatanejo earthquake, over this segment of the plate boundary. Of particular interest is the central fault zone of the Playa Azul earthquake, where the stress dropped by more than 80 bars. During the 1985 Michoacan event, two large-size asperities located at both sides of this zone ruptured, and the central
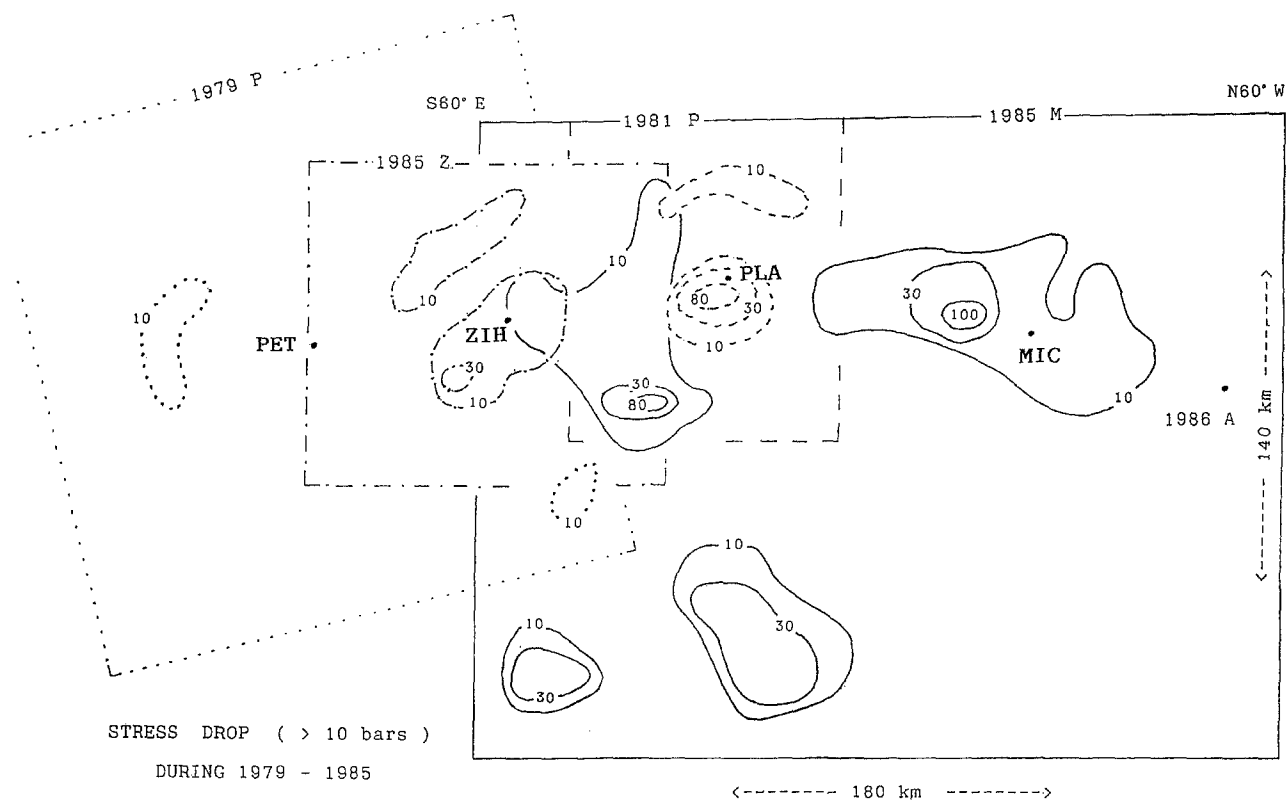
Figure 7.   Zones of positive stress drop higher than 10 bars projected on the fault planes of four large, thrust earthquakes: 1979 Petatlan, 1981 Playa Azul, 1985 Michoacan, and 1985 Zihuatanejo earthquakes. Contours with different symbols represent dynamic stress drop (in bars) during the four earthquakes. Small solid circles indicated by PET, PLA, MIC, and ZIH are the hypocenters of these earthquakes.

zone did not see any more stress drop but still slipped due to the rupture of the two asperities. Thus, reslip occurred on several zones, and new slip took place even in negative stress-drop zones during these earthquakes. These fault slips may be regarded as free slips forced by the failure of a few major asperities with medium to high stress drop. The foregoing definition of "asperity" differs from that often used in previous studies depending on fault slip or moment release (e.g., Kanamori, 1981; Ruff and Miller, 1994). Because these asperities appear to be located near the northern extension of the Orozco Fracture Zone, it is likely that all four large earthquakes might be related with the subduction of this fracture zone with the Cocos–North American plate convergence, as have been suggested by Ruff and Miller (1994).

Figure 8 shows the contours of zero stress drop separating the positive and negative stress-drop zones or the zones of stress decrease and increase after each of the four events (see notations in figure caption). Although these zones overlap each other and appear rather complicated, we notice some features. The increase of stress due to the 1979 Petatlan earthquake (+pe) had been prepared in part of the 1985 Zihuatanejo fault zone, the stress increase due to the 1981 Playa Azul earthquake (+pl) should have been identified around the western large-size asperity of the 1985 Mi-

choacan event, and the increase of stress due to the Michoacan event (+m) had appeared in the eastern part of the Zihuatanejo fault zone. One of the large aftershocks, the 1986 event ($Ms = 7.0$), took place in the northwest zone (+m) outside the major asperity of the Michoacan earthquake. Thus, there is the possibility that the increase of stress due to these large events could contribute, to some extent, to trigger the subsequent earthquakes.

Temporal variations of shear stress at five selected points B, D, E, PLA, and ZIH during the 8 yr from 1979 to 1986 are shown in Figure 9. During the interseismic periods, the shear stress should slowly increase due to the loading of tectonic stress coming from the convergence between the Cocos and North America plates. If we take into consideration the rate of convergence ranging between 5.5 cm/yr (near 104.5° W) and 8.0 cm/yr (near 91.5° W) (Singh and Mortera, 1991), assuming the width of strong interface coupling to be about 60 km (see Fig. 1), the secular rate of stress increase would be about 0.35 to 0.50 bars/yr, which is implicitly included in broken lines in Figure 9. Small rapid rise of the stress just before its large drop at the time of the earthquakes (2), (3), and (4) indicates the strength excess due to the approach of the rupture front toward these points. It is interesting to note that the stress level had increased to
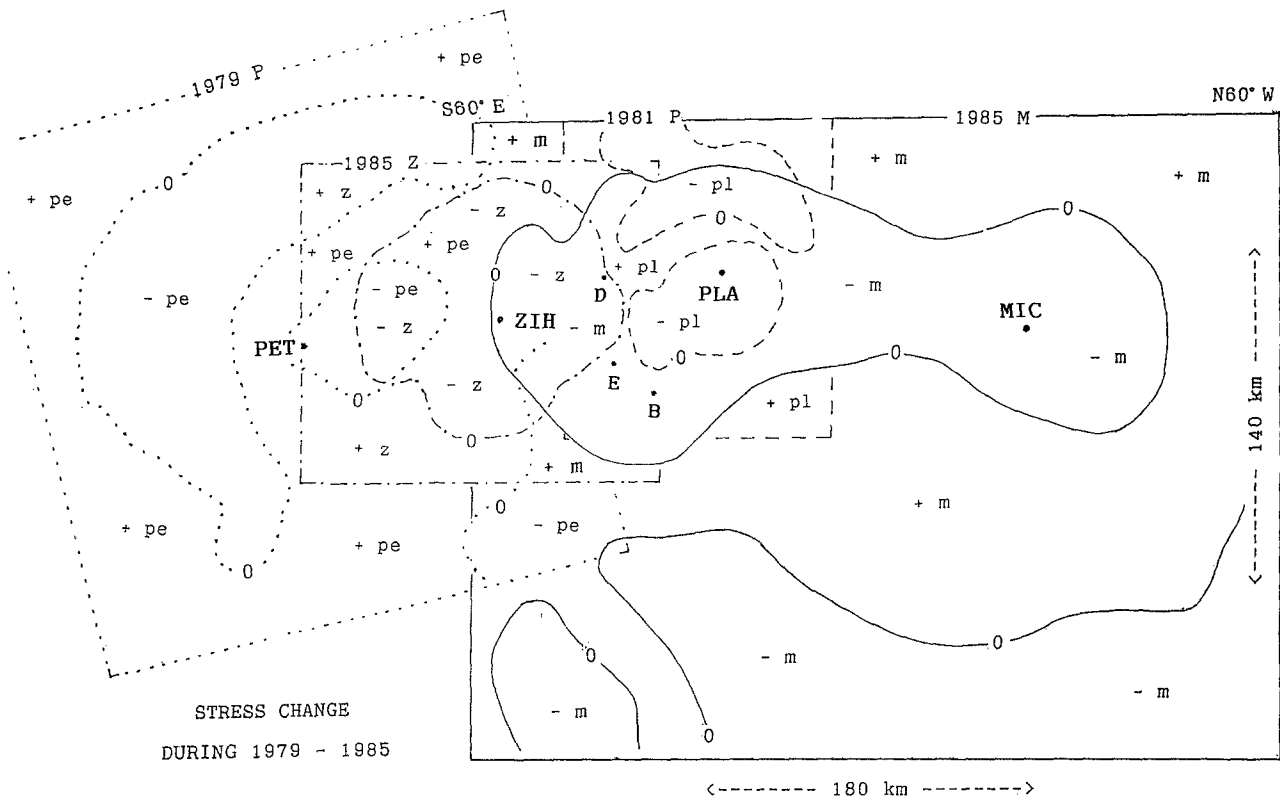
Figure 8.   Contours of zero stress drop separating the positive stress drop (stress decrease) and negative stress drop (stress increase) zones. +pe and −pe: zones of stress increase and decrease due to the Petatlan earthquake; +pl and −pl: zones of stress increase and decrease due to the Playa Azul earthquake; +m and −m: zones of stress increase and decrease due to the Michoacan earthquake; and +z and −z: zones of stress increase and decrease due to the Zihuatanejo earthquake. For symbols PET, PLA, MIC, and ZIH, refer to Figure 7.

an appreciable extent at three points B, E, and ZIH several years prior to the largest 1985 Michoacan earthquake.

Discussion

We would like to point out that several large-size asperities have been ruptured successively in time so as to fill unbroken gaps on the plate interface in and near the Michoacan segment. There remain a few questions, however, as to why the 1981 Playa Azul fault zone ruptured as the second large event following the 1979 Petatlan earthquake, while the 1985 Zihuatanejo fault zone just adjacent to the first event ruptured at the fourth stage, and why the dynamic rupture from each of the large earthquakes has been arrested somewhere between the adjacent fault zones. One possible explanation would be that there was long-wavelength variations of the coupling strength of the interface between the subducting and overriding plates, which might be attributed to some geometrical configurations, with the initial shear stress being distributed just below the strength level. Suppose that the average strength would be the lowest in the

Petatlan region, the second lowest in the Playa Azul region, the second highest in the two Michoacan asperity zones, and the highest in the Zihuatanejo region. It seems likely that the gradual increase of tectonic shear stress due to the plate subduction plus the rapid stress increase due to the dynamic failure of major asperities reached the average strength in the four regions one after another as time progresses. It is possible, however, that if the stress increase solely from the asperity failure cannot overcome the higher strength near the boundaries of the adjacent fault zones, then the dynamic rupture would be arrested there. In this case, the high strength there would work as barriers (e.g., Aki, 1979). The estimates of the strength excess mentioned in this article are not sufficient to solve the above-mentioned problems. These explanations are only speculative at the moment. More theoretical considerations and numerical experiments incorporating long-wavelength lateral variations of strength and stress with their short-wavelength fluctuations (e.g., Mikumo and Miyatake, 1983) might help in understanding these problems as well as temporal and spatial distributions of aftershock generation.
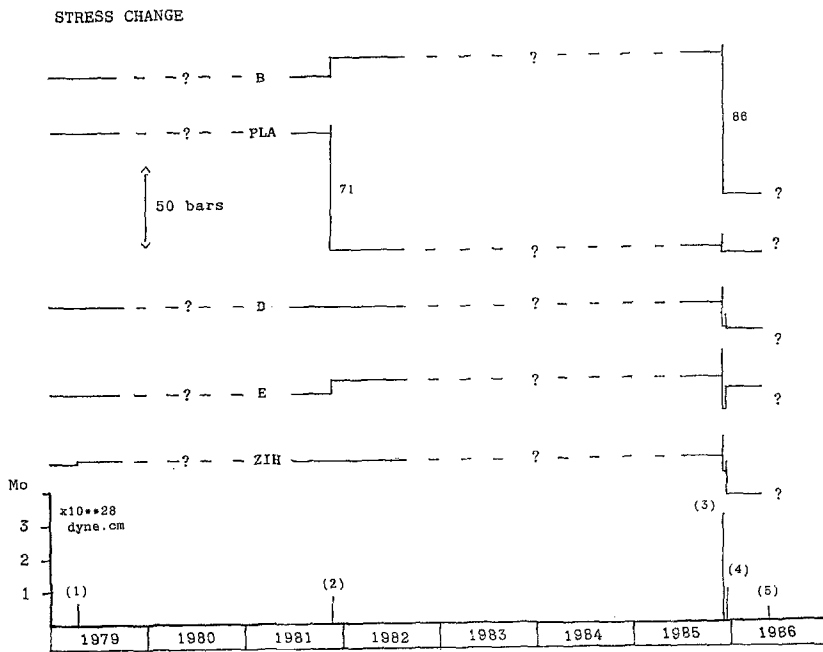
Figure 9. Temporal variations of shear stress at five selected points, B, D, E, PLA, and ZIH on the fault zones (see Fig. 8) during 1979 to 1986. Earthquake numbers (1), (2), (3), (4), and (5) refer to Table 1. M_0 indicates the seismic moment of each earthquake.

Conclusions

We have investigated the spatial and temporal variations of shear stress due to the successive failures of an extensive segment of the Cocos–North America plate boundary during a sequence of large interplate earthquakes that occurred in 8 yr from 1979 to 1986. The sequence included the 1979 Petatlan ($Ms = 7.6$), the 1981 Playa Azul ($Ms = 7.3$), 1985 Michoacan ($Ms = 8.1$), and the 1985 Zihuatanejo ($Ms = 7.6$) earthquakes, all of which had underthrust faulting mechanisms with low dip angles and shallow source depths. For this purpose, we have developed complete 3D dynamic rupture models for these earthquakes, incorporating their shallowly dipping faults rupturing parts of the interface between the subducting and overriding plates, which are embedded in a horizontally layered structure. In these models, some of the kinematic fault parameters previously derived from waveform inversion were used as observational constraints. The spatial distribution of dynamic stress drop and strength excess over the fault have been calculated for each of these earthquakes through an iterative inversion procedure.

It was revealed that heterogeneous stress change over the fault plane of each earthquake came from the failure of a few patchlike, major asperities with medium to high stress drop and from stress increase between and around these asperities. During the first 1979 Petatlan earthquake, two asperities in the fault zone located to the southeast of the Michoacan segment were ruptured, and two asperities in the central zone of the segment were also ruptured during the 1981 Playa Azul earthquake with a maximum stress drop higher than 80 bars. These ruptures have increased shear stress in the zone between the two events and in the northwestern zone of the 1981 event. The 1985 Michoacan earth-

quake ruptured two large-size asperities located at both sides of the 1981 event with maximum stress drops of 80 to 100 bars and two more asperities in the downdip fault section. The stress increase due to this largest event appears to have triggered ruptures on two asperities during the large Zihuatanejo aftershock in the southeastern adjacent region. A possible explanation for the sequence of events is that the increase in stress moves to adjacent regions closer the the critical failure stress and, hence, closer to the time of failure. It was also found that their aftershocks took place mainly in the zones of stress increase outside major asperities, whereas only small numbers of aftershocks occurred within and near the high stress-drop zones. This may be more evidence indicating the increase and decrease of stress due to the mainshocks. It should be mentioned that several major asperities that existed on this segment but not overlapped by each other have been ruptured successively so as to fill unbroken gaps on the plate interface. In the Mexican subduction zone, the stress change caused by the previous earthquake seems to have dominant effects on the subsequent events.

Acknowledgments

References

Aki, K. (1979). Characterization of barriers on an earthquake fault, *J. Geophys. Res.* **84,** 6140–6148.

Anderson, J. G., P. Bodin, J. Brune, J. Prince, S. K. Singh, R. Quaas, M. Onate, and E. Mena (1986). Strong ground motion and source mechanism of the Mexico earthquake of September 19, 1985, *Science* **233,** 1043–1049.

Astiz, L., H. Kanamori, and H. Eissler (1987). Source characteristics of earthquakes in the Michoacan seismic gap in Mexico, *Bull. Seism. Soc. Am.* **77,** 1326–1346.

Beroza, G. and T. Mikumo (1996). Short slip duration in dynamic rupture in the presence of heterogeneous fault properties, *J. Geophys. Res.* **101,** 22449–22460.

Chael, E. P. and G. S. Stewart (1982). Recent large earthquakes along the Middle American Trench and their implications for the subduction process, *J. Geophys. Res.* **87,** 329–338.

DeMets, C., R. G. Gordon, D. F. Argus, and S. Stein (1990). Current plate motions, *Geophys. J. Int.* **101,** 425–478.

Dziewonski, A. M. and J. H. Woodhouse (1983). An experiment in systematic study of global seismicity: centroid moment tensor solutions for 201 moderate and large earthquakes of 1981, *J. Geophys. Res.* **88,** 3247–3271.

Dziewonski, A. M. and H. H. Woodhouse (1986). Centroid-moment tensor solutions for July–December 1985, *Phys. Earth Planet. Interiors* **42,** 205–214.

Eissler, H., L. Astiz, and K. Kanamori (1986). Tectonic setting and source parameters of the September 19, 1985 Michoacan, Mexico earthquake, *Geophys. Res. Lett.* **13,** 569–572.

Ekstrom, G. and A. Dziewonski (1986). A very broad band analysis of the Michoacan, Mexico earthquake of September 19, 1985, *Geophys. Res. Lett.* **13,** 605–608.

Fukuyama, E. and T. Mikumo (1993). Dynamic rupture analysis: inversion for the source process of the 1990 Izu-Oshima, Japan earthquake (M6.5), *J. Geophys. Res.* **98,** 6529–6542.

Havskov, J., S. K. Singh, E. Nava, T. Dominguez, and M. Rodriguez (1983). Playa Azul, Michoacan Mexico earthquake of 25 October 1981 (Ms = 7.3), *Bull. Seism. Soc. Am.* **73,** 449–457.

Houston, H. and H. Kanamori (1986). Source characteristics of the 1985 Michoacan, Mexico earthquake at short periods, *Geophys. Res. Lett.* **13,** 597–600.

Ide, S. and M. Takeo (1996). The dynamic rupture process of the 1993 Kushiro-oki earthquake, *J. Geophys. Res.* **101,** 5661–5675.

Kanamori, H. (1981). The nature of seismicity patterns before large earthquakes, in *Earthquake Prediction—An International Review, Maurice Ewing Series 4,* D. W. Simpson and P. G. Richards (Editors), American Geophysical Union, Washington, D.C., 1–19.

LeFevre, L. V. and K. C. McNally (1985). Stress distribution and subduction of aseismic ridges in the middle America subduction zone, *J. Geophys. Res.* **90,** 4495–4510.

Levander, A. R. (1985). Use of the telegraphy equation to improve absorbing boundary efficiency for fourth-order acoustic wave finite difference scheme, *Bull. Seism. Soc. Am.* **75,** 1847–1852.

McNally, K. C. and J. B. Minster (1981). Nonuniform seismic slip rates along the middle America trench, *J. Geophys. Res.* **86,** 4949–4959.

Mendez, A. J. and J. G. Anderson (1991). The temporal and spatial evolution of the 19 September 1985 Michoacan earthquake as inferred from near-source ground-motion records, *Bull. Seism. Soc. Am.* **81,** 844–861.

Mendoza, C. (1993). Coseismic slip of two large Mexican earthquakes from teleseismic body waveforms: implications for asperity interaction in the Michoacan plate boundary segment, *J. Geophys. Res.* **98,** 8197–8210.

Mendoza, C. (1995). Finite-fault analysis of the 1979 March 14 Petatlan, Mexico, earthquake using teleseismic P waveforms, *Geophys. J. Int.* **121,** 675–683.

Mendoza, C. and S. Hartzell (1988). Inversion for slip distribution using

teleseismic P waveforms: North Palm Springs, Borah Peak, and Michoacan earthquakes, *Bull. Seism. Soc. Am.* **78,** 1092–1111.

Mendoza, C. and S. Hartzell (1989). Slip distribution of the 19 September 1985 Michoacan, Mexico, earthquake: near-source and teleseismic constraints, *Bull. Seism. Soc. Am.* **79,** 655–669.

Mikumo, T. and T. Miyatake (1983). Numerical modelling of space and time variations of seismic activity before major earthquakes, *Geophys. J. R. Astr. Soc.* **14,** 559–583.

Mikumo, T. and T. Miyatake (1993). Dynamic rupture processes on a dipping fault, and estimates of stress drop and strength excess from the results of waveform inversion, *Geophys. J. Int.* **112,** 481–496.

Mikumo, T. and T. Miyatake (1995). Heterogeneous distribution of dynamic stress drop and relative fault strength recovered from the results of waveform inversion: 1984 Morgan Hill, California, earthquake, *Bull. Seism. Soc. Am.* **85,** 178–193.

Mikumo, T., K. Hirahara, and T. Miyatake (1987). Dynamical fault rupture processes in heterogeneous media, *Tectonophysics* **144,** 19–36.

Mikumo, T., M. Santoyo, and T. Miyatake (1998). Slip duration in dynamic rupture of large thrust earthquakes (in preparation).

Miyatake, T. (1992). Reconstruction of dynamic rupture process of an earthquake with constraints of kinematic parameters, *Geophys. Res. Lett.* **19,** 349–352.

Okada, Y. (1993). Internal deformation due to shear and tensile faults in a half-space, *Bull. Seism. Soc. Am.* **82,** 1018–1040.

Pardo, M. and G. Suarez (1995). Shape of the subducted Rivera and Cocos plates in southern Mexico: seismic and tectonic implications, *J. Geophys. Res.* **100,** 12357–12373.

Priestley, K. F. and T. G. Masters (1986). Source mechanism of the September 19, 1985 Michoacan earthquake and its implications, *Geophys. Res. Lett.* **13,** 601–604.

Riedesel, M. A., T. H. Jordan, A. F. Sheeman, and P. G. Silver (1986). Moment tensor spectra of the 19 Sept. 85 and 21 Sept. 85 Michoacan, Mexico, earthquake, *Geophys. Res. Lett.* **13,** 609–612.

Ruff, L. J. and A. D. Miller (1994). Rupture process of large earthquakes in the northern Mexico subduction zone, *Pageoph* **142,** 102–171.

Singh, S. K. and F. Mortera (1991). Source-time functions of large Mexican subduction earthquakes, morphology of the Benioff zone, age of the plate and their tectonic implications, *J. Geophys. Res.* **96,** 21487–21502.

Singh, S. K., L. Astiz, and J. Havskov (1981). Seismic gaps and recurrence periods of large earthquakes along the Mexican subduction zone: a re-examination, *Bull. Seism. Soc. Am.* **71,** 827–843.

Singh, S. K., T. Dominguez, R. Castro, and M. Rodriguez (1984). P waveforms of large shallow earthquakes along the Mexican subduction zone, *Bull. Seism. Soc. Am.* **74,** 2135–2156.

Singh, S. K., E. Mena, and R. Castro (1988). Some aspects of source characteristics of the 19 September 1985 Michoacan earthquake and ground motion amplification in and near Mexico City from strong motion data, *Bull. Seism. Soc. Am.* **78,** 451–477.

Stolte, C., K. C. McNally, J. Gonzales-Ruiz, G. W. Smith, A. Reyes, C. Rebollar, L. Munguia, and I. Mendoza (1986). Fine structure of a post-failure Wadati-Benioff zone, *Geophys. Res. Lett.* **13,** 577–580.

Suarez, G. and O. Sanchez (1996). Shallow depth of seismogenic coupling in southern Mexico: implications for the maximum size of earthquakes in the subduction zone, *Phys. Earth Planet. Interiors* **93,** 53–61.

UNAM Seismology Group (1986). The September 1985 Michoacan earthquakes: aftershock distribution and history of rupture, *Geophys. Res. Lett.* **13,** 573–576.

Valdez, C. and R. P. Meyer (1996). Seismic structure between the Pacific coast and Mexico City from the Petatlan earthquake (Ms = 7.6) aftershocks, *Geofis. Int.* **35,** 377–401.

Valdez, C., R. P. Meyer, and R. Zuniga, J. Havskov, and S. K. Singh (1982). Analysis of the Petatlan aftershocks: numbers, energy release and asperities, *J. Geophys. Res.* **87,** 8519–8527.

Valdez, C. M., W. D. Mooney, S. K. Singh, R. P., Meyer, C. Lomnitz, J. H. Luetgert, C. E. Helsley, B. T. R. Lewis, and M. Mena (1986).

Crustal structure of Oaxaca, Mexico, from seismic refraction exper-
iments, *Bull. Seism. Soc. Am.* **76,** 547–563.

Yomogida, K. (1988). Crack-like rupture processes observed in near-fault
strong motion data, *Geophys. Res. Lett.* **15,** 1223–1226.

Zhang, J. and H. Kanamori (1988). Depth of large earthquakes determined
from long-period Rayleigh waves, *J. Geophys. Res.* **93,** 4850–4868.

Instituto de Geofisica
Universidad Nacional Autonoma de Mexico
Mexico 04510 D.F., Mexico
E-mail: mikumo@ollin.igeofcu.unam.mx
  (T.MK., M.A.S.)

Earthquake Research Institute
University of Tokyo
Tokyo 113, Japan
  (T.MY.)